

Rotating vortices in two-dimensional inhomogeneous strongly coupled dusty plasmas: shear and spiral-density waves

Vikram S. Dharodi^{1, a)}

Mechanical Engineering, Michigan State University, East Lansing, Michigan 48824, USA.

(Dated: 9 June 2020)

Dusty plasma experiments can be performed quite easily in strong coupling regime. In our previous work [Phys. Plasmas 21, 073705 (2014)], we numerically explored such plasmas with constant density and observed the transverse shear (TS) waves from a rotating vortex. Laboratory dusty plasmas are good examples of homogeneous plasmas however heterogeneity (e.g. density, temperature, charge) may be due to the existence of voids, different domains with different orientations, presence of external forces like magnetic and/or electric, size/charge imbalance, etc. Here, we examine how the density heterogeneity in dusty plasmas responds to the circularly rotating vortex monopoles, namely smooth and sharp cut-off. For this purpose we have carried out a series of two-dimensional viscoelastic fluid simulations in the framework of generalized hydrodynamics (GHD) fluid model. The rotating vortices are placed at the interface of two incompressible fluids with different densities. The smooth rotating vortex causes two things: First, the densities are stretched to form the spiral density waves; secondly, the TS waves propagate radially into the surrounding media according to the shear wave speed. We notice that the spiral density arms are distinguishable in the early time while later get smeared out. The sharp rotating vortex creates sharp shear flows which in turn favor the Kelvin-Helmholtz (KH) instability across the interfaces. In such flows for the GHD system, the interplay between the emitted TS waves and the vortices of KH instability distorts the formation of the regular spiral density arms around the rotor.

^{a)}Electronic mail: dharodiv@msu.edu

I. INTRODUCTION

A typical fluid/turbulent flow contains a wide variety of coherent structures¹ like rotating monopoles and tripoles^{2,3}, propagating and merging dipoles⁴. It becomes important to understand how such types of structures encounter the density and/or temperature gradient in a medium, which may cause the formation of different kinds of waves like acoustic⁵⁻⁷, shock⁸⁻¹⁰, spiral^{11,12}, transverse¹³⁻¹⁸ and fluid instabilities like Kelvin-Helmholtz^{19,20}, Rayleigh-Taylor^{21,22}. Laboratory dusty plasmas are good examples of homogeneous plasmas however heterogeneity (e.g. density, temperature, charge) may be due to the existence of voids, different domains with different orientations, presence of external forces like magnetic and/or electric, size/charge imbalance, etc. Our objective here is to understand how the density heterogeneity in a strongly coupled state responds to the coherent structures (here, rotating vortex monopoles). For this purpose we specifically here consider the case of two-dimensional (2D) dusty plasmas. The motivational factors that induce us to choose such 2D plasmas are: 2D dusty plasmas are favored in laboratory experiments²³⁻²⁹ and simulations^{10,30-33}, dusty plasmas can exist in strong coupling state quite easily because of high charged dust particles, and in dusty plasmas a coherent structure can survive for a longer time than in a hydrodynamic fluid (viscosity shows pure damping effect) because the effect of viscosity gets reduced due to the presence of elasticity³⁴. Thus, in dusty plasmas, a long-lived coherent structure can act as a driving force in order to understand its collective response for a long-time duration without much dissipation.

Strongly coupled dusty plasmas (SCDPs) behave like viscoelastic mediums cause to support the existence of both incompressible transverse shear and compressible longitudinal modes³⁵⁻³⁷. Here, we have modeled this medium using well-known phenomenological generalized hydrodynamic (GHD) fluid model which takes into account both types of modes^{38,39}. It should be noted that a fluid model focuses on a situation where the spacial scales in dusty plasmas are supposed to be about an order of magnitude larger than the interparticle distance while fails as soon as the grainy structure becomes important. To study the effect of inhomogeneity on exclusive transverse modes and to avoid the possible coupling with longitudinal mode, we consider the incompressible limit of the dusty plasma. Theoretically, the existence of transverse modes in dusty plasma medium has been predicted in^{13,14,16}. Schmidt *et al.*¹⁵ showed such transverse modes in molecular dynamic simulations. Nunomura *et al.*⁴⁰, Pramanik *et al.*⁴¹ and Pintu *et al.*⁴² have also observed transverse modes in dusty plasma experiment. Using GHD model, the shear waves in a nonuni-

form dusty plasma has been studied in^{43,44}. Apart from the shear waves, a nonuniform dusty plasma under stretching due to a driving force may cause to support the spiral waves. Recently, Sandeep *et al.* reported the existence of spiral waves in SCDPs at particle level using molecular-dynamics simulations in⁴⁵ and at continuum level using the GHD model in⁴⁶. In incompressible fluid simulations, Li *et al.*⁴⁷ found the multi-armed spiral waves in a slowly rotating fluid, driven by a radial unstable temperature gradient. The existence of spiral waves are observed in various biological systems like retinal spreading depression⁴⁸, cardiac muscle⁴⁹, and *Xenopus* oocyte calcium waves⁵⁰. Apart from the biology, the understanding of spiral waves are important in mathematics, and physics, because the spiral wave formation takes place in nonlinear nonequilibrium systems⁵¹. A rotating galaxy is a good example of the large scale spirals⁵².

In our previous work⁵³, we explored the constant density dusty plasmas in an incompressible limit of GHD model and observed the transverse shear (TS) waves due to the shear flow induced from a rotating monopole vortex. In the current work, we use same model where the smooth and sharp cut-off rotating vortices are placed at the interface of two incompressible fluids with different densities. The smooth rotating vortex at the interface causes two things: first, this rotating vortex convects material from the higher density part to the lower density part and vice versa which leads to the formation of spiral density waves, and second, locally introduce a shear flow. This shear flow is the source for the shear waves. These waves propagate into the surrounding media according to the shear wave speed where the waves travel a smaller distance in higher density part than in lower density part in the same time interval. The sharp rotating vortex creates sharp shear flows which favor the Kelvin-Helmholtz (KH) instability across their interfaces along with the TS waves. In such flows the interplay between the emitted TS waves and the vortices of KH instability occurs which in turn distorts the formation of the regular spiral density waves around the rotor. Because of incompressible limit ($\nabla \cdot \vec{v}_d = 0$), to observe the spiral density waves the initial density profile must have a radially varying component to the rotating vortex. Although, here, the density inhomogeneity has been introduced hypothetically (in order to identify the TS waves) for simulation but the presented results can be easily generalized to any typical SCDP experiment having realistic density inhomogeneity *e.g.*, sech type, parabolic type, etc. and by locating the driving vortex at the required place.

This paper is organized as follows. In Section II, we discuss the incompressible limit of GHD (i-GHD) model used for the SCDPs and drive an analytical linear wave equation. In Section III, we discuss how the simulations are initialized and analyse the dynamical response of the

density heterogeneity to the circularly rotating vortex monopoles, particularly smooth and sharp cut-off. In the subsection III A, we numerically observe that a smooth rotating vorticity profile emits cylindrical TS waves and also causes to rolling-up the densities to form the spiral density waves. In the subsection III B, for sharp rotating flows, the interplay between the emitted TS waves and the vortices of KH instability occurs which in turn distorts the formation of the spiral density waves around the rotor. Finally, in Section IV, we discuss our results and offer concluding remarks.

II. INCOMPRESSIBLE GENERALIZED HYDRODYNAMICS (I-GHD) FLUID MODEL

Generalized hydrodynamic fluid model^{38,54} is a phenomenological model which is used to study the SCDPs, both analytically as well as numerically^{38,39,53,55}. GHD model treat dusty plasma as a viscoelastic fluid in which the coupling strength is proportional to the ratio of η/τ_m ³⁴, η is the shear viscosity coefficient and τ_m is the relaxation time parameter. The parameters η and τ_m are supposed to be empirically related to each other^{38,56}. This model supports both the existence of incompressible transverse shear and compressible longitudinal modes. Here, we separate out the compressibility effects altogether and the incompressible limit of the GHD (i-GHD) set of equations has been obtained. In the incompressible limit the Poisson equation is replaced by the quasi-neutrality condition and charge density fluctuations are ignored. The derivation of the reduced equations has been discussed in detail in our earlier papers^{53,55} along with the procedure of its numerical implementation and validation. The coupled set of continuity and momentum equations for the dust fluid can be written as:

$$\frac{\partial \rho_d}{\partial t} + \nabla \cdot (\rho_d \vec{v}_d) = 0, \quad (1)$$

$$\begin{aligned} & \left[1 + \tau_m \left(\frac{\partial}{\partial t} + \vec{v}_d \cdot \nabla \right) \right] \\ & \left[\rho_d \left(\frac{\partial \vec{v}_d}{\partial t} + \vec{v}_d \cdot \nabla \vec{v}_d \right) + \alpha \nabla \rho_d + \rho_c \nabla \phi_d \right] \\ & = \eta \nabla^2 \vec{v}_d, \end{aligned} \quad (2)$$

respectively and the incompressible condition is given as

$$\nabla \cdot \vec{v}_d = 0. \quad (3)$$

Here, the variables ρ_d and ρ_c , \vec{v}_d and ϕ_d are the dust mass density, dust charge density, dust fluid velocity and dust charge potential, respectively. The pressure is simply a function of density through equation of state and α represents the square of sound speed of the medium. The time, length, velocity and potential are normalised by inverse of dust plasma frequency $\omega_{pd}^{-1} = (4\pi(Z_d e)^2 n_{d0}/m_{d0})^{-1/2}$ and plasma Debye length $\lambda_d = (K_B T_i / 4\pi Z_d n_{d0} e^2)^{1/2}$, $\lambda_d \omega_{pd}$ and $Z_d e / K_B T_i$ respectively. The parameters m_d , T_i and K_B are the dust grain mass, ion temperature and Boltzmann constant respectively. Z_d is the charge on each dust grain with no consideration of charge fluctuation. The number density n_d is normalised by the equilibrium value n_{d0} .

A. Transverse wave equation

If we take the curl of above momentum Eq. (2) and keep the linearized terms only, for the moment, the density is constant *i.e* $\rho_d(x, y, t) = \rho_d$, we immediately get the equation

$$\left[1 + \tau_m \frac{\partial}{\partial t} \right] \left[\frac{\partial \vec{\xi}}{\partial t} \right] = \frac{\eta}{\rho_d} \nabla^2 \vec{\xi} \quad (4)$$

$\vec{\xi} = \vec{\nabla} \times \vec{v}_d$ is the vorticity, normalised with dust plasma frequency. In limit $\tau_m \frac{\partial}{\partial t} \geq 1$, where the memory effects are strong, we get

$$\frac{\partial^2 \vec{\xi}}{\partial t^2} = v_p^2 \nabla^2 \vec{\xi}. \quad (5)$$

This wave Eq. (5) suggests that i-GHD model support the transverse waves moving with phase velocity

$$v_p = \sqrt{\eta / \rho_d \tau_m}. \quad (6)$$

Equation (5) also evident that the form of a wave is determined by its source. Let's suppose that we have a line source, the wavefronts will be cylindrical. So, the wave Eq. (5) in cylindrical coordinates will become

$$\frac{\partial^2 \xi_z(\vec{r}, t)}{\partial t^2} = v_p^2 \left(\frac{\partial^2 \xi_z(\vec{r}, t)}{\partial r^2} + \frac{1}{r} \frac{\partial \xi_z(\vec{r}, t)}{\partial r} \right). \quad (7)$$

Here, $r = (x^2 + y^2)^{1/2}$. The solution are Bessel functions which for large r approach asymptotically⁵⁷ to

$$\xi_z(\vec{r}, t) = \xi_z(\vec{r}, \omega) \approx \frac{\xi_{z0}}{\sqrt{r}} e^{-j\omega t} \quad (8)$$

Here, angular frequency $\omega = k v_p$, and k is wavenumber. The associated wavefronts are cylindrical which propagate radially outward at the phase velocity $v_p = \omega/k = \sqrt{\eta/\rho_d \tau_m}$ and their amplitude decrease as $1/\sqrt{r}$. If the wavefront emerging/collapsing from/into a point is spherical, their amplitude must attenuate as $1/r$. A planar source will produce plane wavefronts traveling with a constant amplitude *i.e.* the wave does not attenuate. The amplitude scaling of these wavefronts is related to the energy conservation consideration. Note that the present simulations have been carried out in two-dimensional (x-y plane) which is the plane of rotation for vorticity structures. So, a numerically expected transverse wave should meet the conditions for the cylindrical case.

III. RESULTS DISCUSSION AND NUMERICAL SIMULATION

For the numerical simulation the generalized momentum Eq. (2) has been expressed as a set of following two coupled convective equations,

$$\rho_d \left(\frac{\partial \vec{v}_d}{\partial t} + \vec{v}_d \cdot \nabla \vec{v}_d \right) + \alpha \nabla \rho_d + \rho_c \nabla \phi_d = \vec{\psi} \quad (9)$$

$$\frac{\partial \vec{\psi}}{\partial t} + \vec{v}_d \cdot \nabla \vec{\psi} = \frac{\eta}{\tau_m} \nabla^2 \vec{v}_d - \frac{\vec{\psi}}{\tau_m}. \quad (10)$$

For our considered 2D system of equations the above variables vary in x and y directions *i.e.* $\vec{\psi}(x, y)$, $\vec{v}_d(x, y)$, $\rho_d(x, y)$. From Eq. (9) it is clear that the quantity $\vec{\psi}(x, y)$ is the strain created in the elastic medium by the time-varying velocity fields. Let's take the curl of an Eq. (9). Here, the curl of the second (because pressure is a function of density through equation of state, so the curl becomes zero) and third term (as charge density is constant, so the curl becomes zero) vanish. Thus, the final coupled numerical model equations of continuity and momentum equations becomes

$$\frac{\partial \rho_d}{\partial t} + (\vec{v}_d \cdot \nabla) \rho_d = 0, \quad (11)$$

$$\frac{\partial \vec{\psi}}{\partial t} + (\vec{v}_d \cdot \nabla) \vec{\psi} = \frac{\eta}{\tau_m} \nabla^2 \vec{v}_d - \frac{\vec{\psi}}{\tau_m}, \quad (12)$$

$$\frac{\partial \xi_z}{\partial t} + (\vec{v}_d \cdot \nabla) \xi_z = \frac{\partial}{\partial x} \left(\frac{\psi_y}{\rho_d} \right) - \frac{\partial}{\partial y} \left(\frac{\psi_x}{\rho_d} \right). \quad (13)$$

We have used the LCPFCT method (Boris *et al.*⁵⁸) to evolve the coupled set of Eqs. (11), (12) and (13) for various kinds of density profiles. This method is based on a finite difference scheme associate with the flux-corrected algorithm. The velocity at each time step has been updated by

using the Poisson's equation $\nabla^2 \vec{v}_d = -\vec{\nabla} \times \vec{\xi}$. This Poisson's equation has been solved by using the FISPACK⁵⁹. It is point out that in this particular limit, there is nothing specific which suggests that the system corresponds to a strongly coupled dusty plasma. Thus, the results discussed in this paper would in general be relevant to any viscoelastic fluid and not be restricted to the SCDPs.

Numerically, in order to understand the dynamical response of density inhomogeneous SCDPs, we consider two cases of circularly rotating fluid vortex, especially having (A) smooth rotating vortex and consider another which has a (B) sharp cut-off. Boundary conditions are periodic along the x-axis while absorbing in y-direction throughout the entire simulation work.

A. Smooth rotating vortex

In the former case (A), we have considered a system of length $l_x = l_y = 8\pi$ units with sharp interface of density heterogeneity shown in Fig. 1(a), where two incompressible fluids with different constant densities $\rho_d=1$ for $-4\pi \leq y \leq 0$ (lighter) and $\rho_d=2$ for $0 = y \leq 4\pi$ (denser) are positioned side-by-side along the $y=0$ interface.

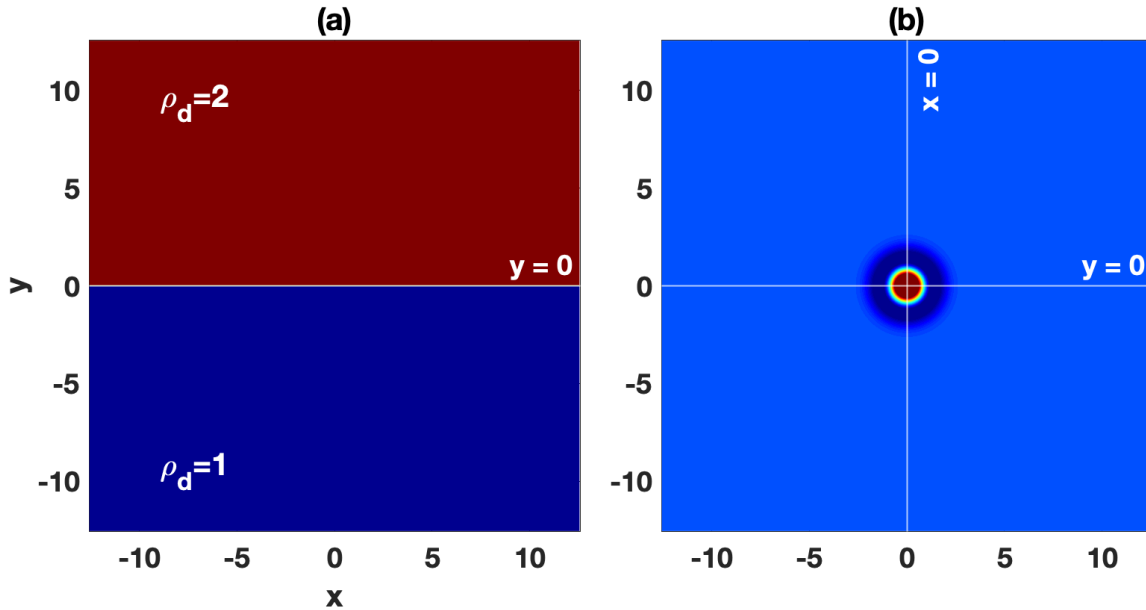


FIG. 1. The initial density and smooth rotating vorticity profiles. (a) Density profile where the lighter fluid is positioned side-by-side to the denser fluid along the $y=0$ interface, and (b) initial profile of the smooth rotating vorticity structure given by Eq. (14).

In interest of density waves and vorticity evolution, the sharp density interface of the medium

has been perturbed through a counter-rotating vorticity structure centered at $(x,y) = (0,0)$, given by

$$\xi_{z0}(x,y,t_0) = \Omega_0(1 - (x^2 + y^2)) \exp(-(x^2 + y^2)), \quad (14)$$

having the velocity components which satisfy the condition of incompressibility $\nabla \cdot \vec{v} = 0$ using $\vec{\xi} = \vec{\nabla} \times \vec{v}$, $v_{x0}(x,y,t_0) = -\phi_0 y \exp(-(x^2 + y^2))$ and $v_{y0}(x,y,t_0) = \phi_0 x \exp(-(x^2 + y^2))$. Here $\Omega_0 = 2\phi_0$ is proportional to the total circulation. This vorticity profile has circular symmetry (ref. Fig. 1(b)).

1. Transverse shear waves

The time evolution of the above vorticity profile for $\Omega_0 = 10$ is shown in Fig. 2 (a), where $\eta = 5$ and $\tau_m = 20$.

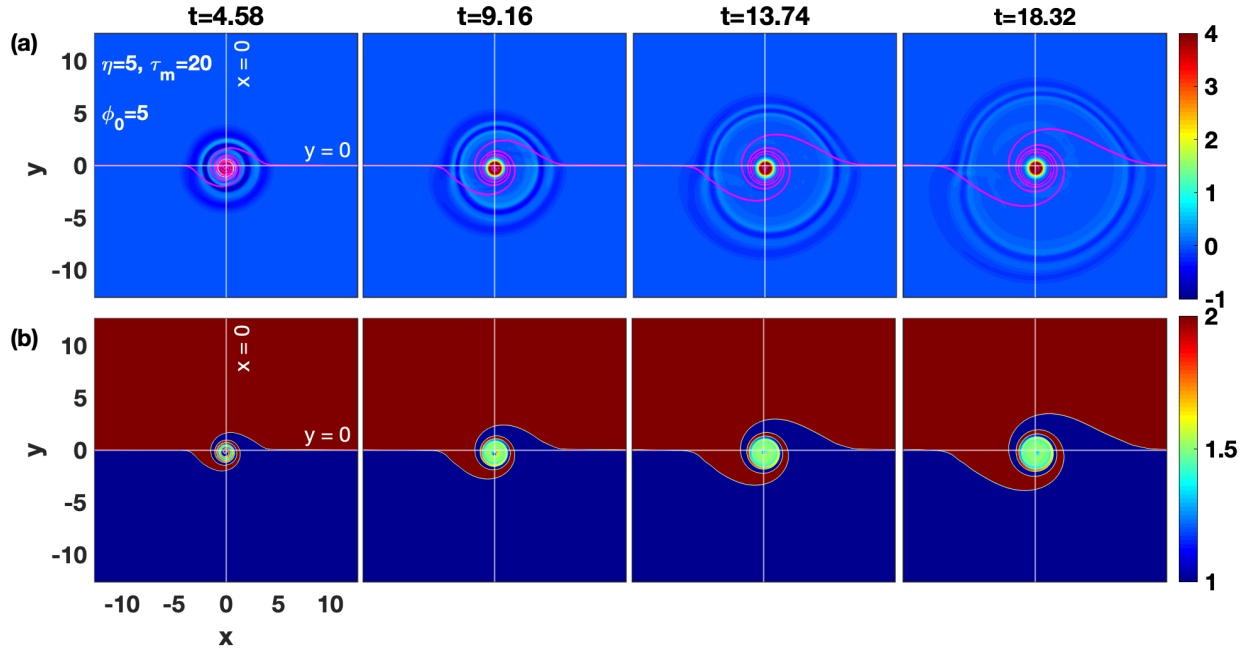


FIG. 2. Time evolution of a counter-rotating circular vorticity profile ($\Omega_0 = 10$) in a medium ($\eta=5$; $\tau_m=20$) where density inhomogeneity is along the interface $y=0$. (a) Evolution of a counter-rotating circular vorticity (Fig. 1(b)), where the magenta color solid line is just the interface of respective density profile; the colorbar indicates the vorticity. In (b) density profile evolution (Fig. 1(a)); the colorbar indicates the density.

From Fig. 2(a), as soon as the vortex starts rotating at the interface induces two things: first, the densities are rolled-up to form the spiral density waves (we will discuss it later), and second, locally introduce a shear flow. This shear flow is the source for the radial shear waves. These

radial waves travel a smaller distance in higher density part than in lower density part in the same time interval. In Fig. 3 we have plotted the positions of a particular wavefront with time along the y-axis for $x = 0$.

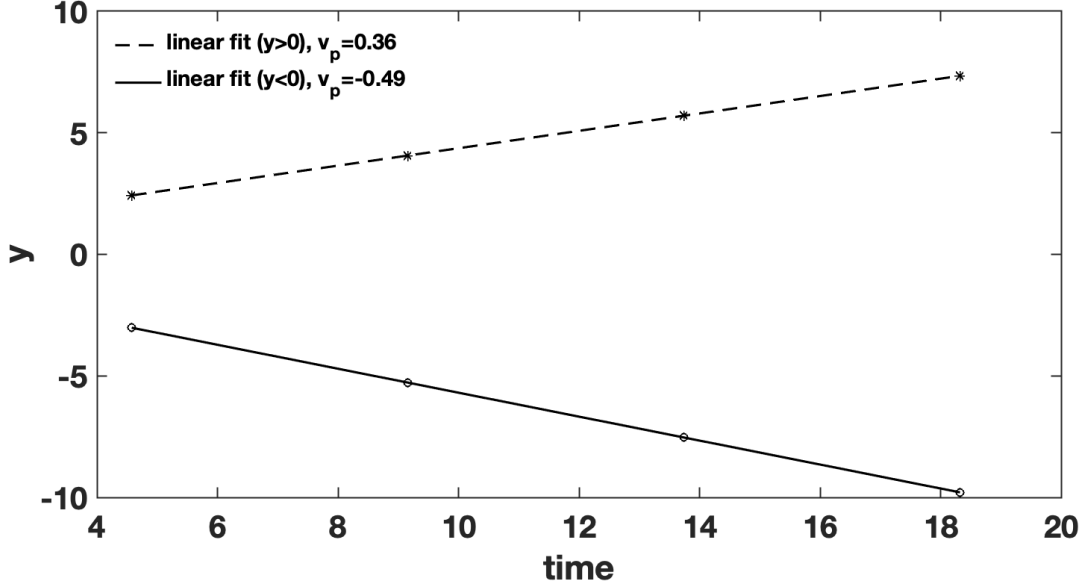


FIG. 3. Position-time graph of a radially propagating wavefront (along the y-axis for $x=0$) observed in Fig. 2(a) for coupling parameter values $\eta=5$; $\tau_m=20$, where v_p is the phase velocity (slope of position-time plot). Here, dotted line is the linear curve fit for the denser side ($y > 0$) and solid line is the linear curve fit for the lighter side ($y < 0$). It is observed that the waves travel faster ($v_p \approx 0.5$) in lighter side while at the slow rate ($v_p \approx 0.35$) in the denser side of the medium which confirms that these emitted waves are TS waves.

In Fig. 3, position-time slope suggests that the phase velocity (v_p) is found to match with Eq. (6) i.e. $v_p \approx 0.35$ for denser side ($\eta=5$; $\tau_m=20$ and $\rho_d=2$ for $y > 0$) and in lighter side $v_p \approx 0.5$ ($\eta=5$; $\tau_m=20$ and $\rho_d=1$ for $y < 0$). It confirms that the emerging waves are the transverse shear (TS) waves. Figure 4 shows the radial fall of amplitude of the emitted TS wave in the both sides (denser and lighter) of the density profile. It is found to match the fall of amplitude with $1/\sqrt{y}$ which meets the requirement of energy conservation for a cylindrical wave (has been discussed in the subsection II A). It confirms that the emitted TS waves have cylindrical shape.

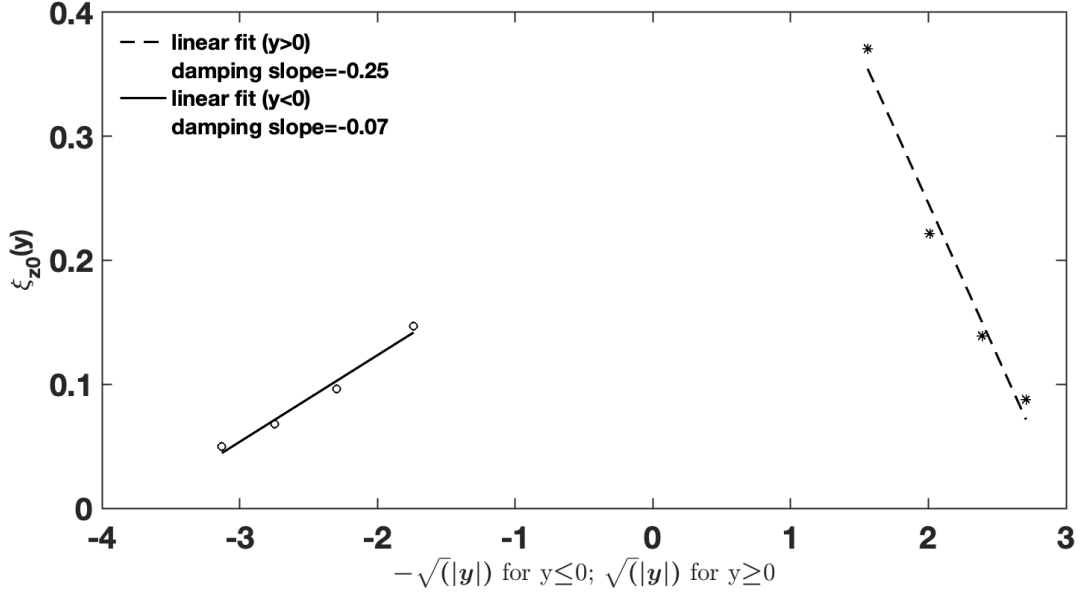


FIG. 4. Amplitude vs. square-root of position of a radially propagating wavefront (along the y-axis for $x=0$, ref. Fig. 2(a)) for the $\eta=5$; $\tau_m=20$. Dotted line for the denser side ($y > 0$) is linear curve fit and solid line for the lighter side ($y < 0$) is linear curve fit. It is observed that the amplitude of a wavefront decreases as $1/\sqrt{y}$ for the moving wavefront i.e. as y increases. It confirms that the emitted TS waves has cylindrical shape.

Hence, both the above observations (Figs. 3 and 4) confirm that these emerging waves are the linear cylindrical TS waves as suggested by analytical Eq. (7) and also indicate the validation of our numerical code. The coupling strength parameter Γ for a dusty plasma is proportional to the cube root of density⁶⁰ which means denser side has larger coupling strength than lighter one. This effect can be noticed from Fig. 2(a) where the TS waves get more clearer/steeper in denser side than lighter one. Furthermore, due the density gradient and the higher speed of TS waves in lighter side than denser, the counter rotating vorticity center gets little shifted towards the low density side and the emerging TS waves are no longer cylindrical symmetric around the center of rotation.

2. Formation and evolution of spiral density waves

After the confirmation of TS waves, let's focus on the evolution of background density profile shown in Fig. 2(b), where the rotating vortex basically convects material from the high denser part to the less dense part and vice versa which results the spiral density arms/waves around the vortex

with time. One of the main advantages of viscoelastic fluids is that a rotating vortex in such media can drive density waves for a long-time duration without much dissipation than in hydrodynamic fluids. A comparative analysis of evolution of vorticity structures in Fig. 2(a) to the density spiral structures in Fig. 2(b) shows that the perturbed density region along the interface follows the radially propagating TS waves and remains confined within the distance traveled by the TS waves at that moment. To make it more clear we have also plotted the interface of respective density profile over the vorticity using a magenta colored solid line in Fig. 2(a). In order to substantiate our observations, we have also simulated two more cases with same background density inhomogeneity, first (Fig. 5(a)) with same rotation rate of vorticity ($\Omega_0 = 10$) but with different values of coupling parameters ($\eta = 2.5$; $\tau_m = 20$) i.e. TS waves travel with less phase velocity and second (Fig. 5(b)) with double rotation rate of vorticity ($\Omega_0 = 20$) but with same values of coupling parameters ($\eta = 5$; $\tau_m = 20$) i.e. TS waves travel with same phase velocity (Fig. 2(a)). It can be seen that these two cases too favor our earlier observation and implies that the spiral waves can be controlled by tweaking the coupling parameter values.

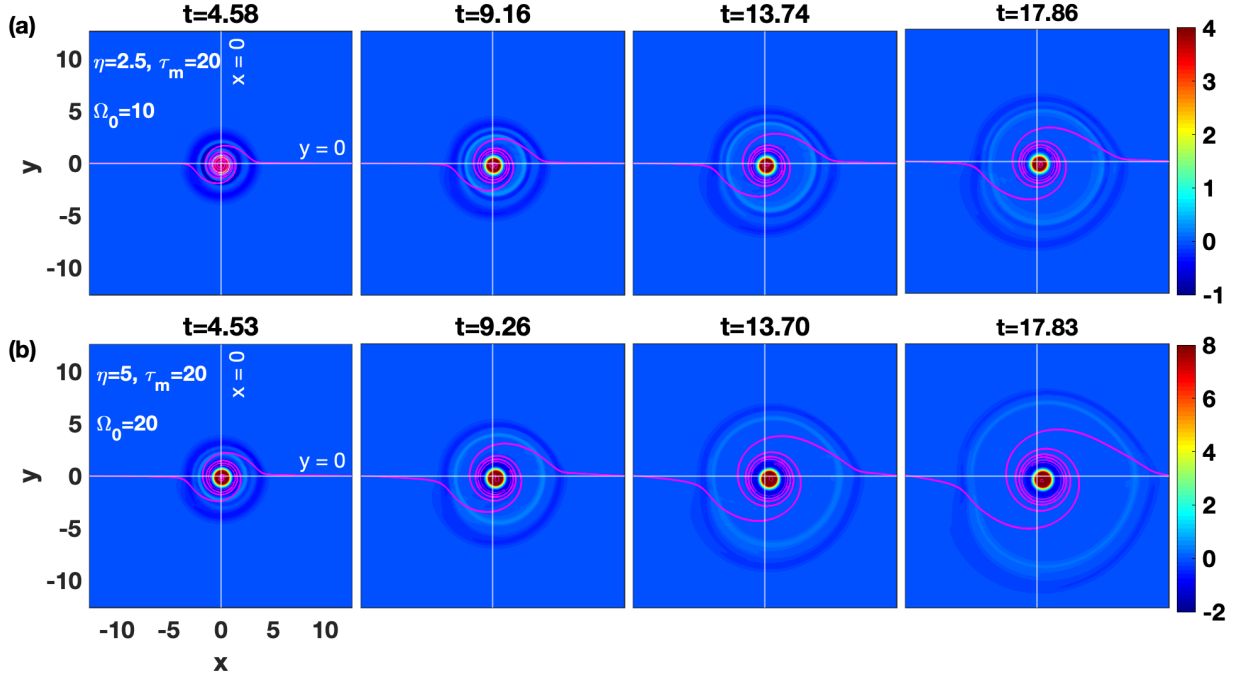


FIG. 5. Time evolution of a rotating circular vorticity profile in a medium of sharp density inhomogeneity along the interface $y=0$, where the line plot (magenta color) represents the density interface over the respective rotating vorticity. (a) $\Omega_0 = 10$ and $\eta = 2.5$; $\tau_m = 20$, and (b) $\Omega_0 = 20$ and $\eta = 5$; $\tau_m = 20$. It is observed that the perturbed density region along the interface follows the radially propagating TS waves and remains confined within the distance traveled by the TS waves at that moment. Conclusion, the impact of spiral waves can be controlled by tweaking the coupling parameter values.

These observations can be visualised more clearly through the zoomed density contour snapshots shown in Fig. 6.

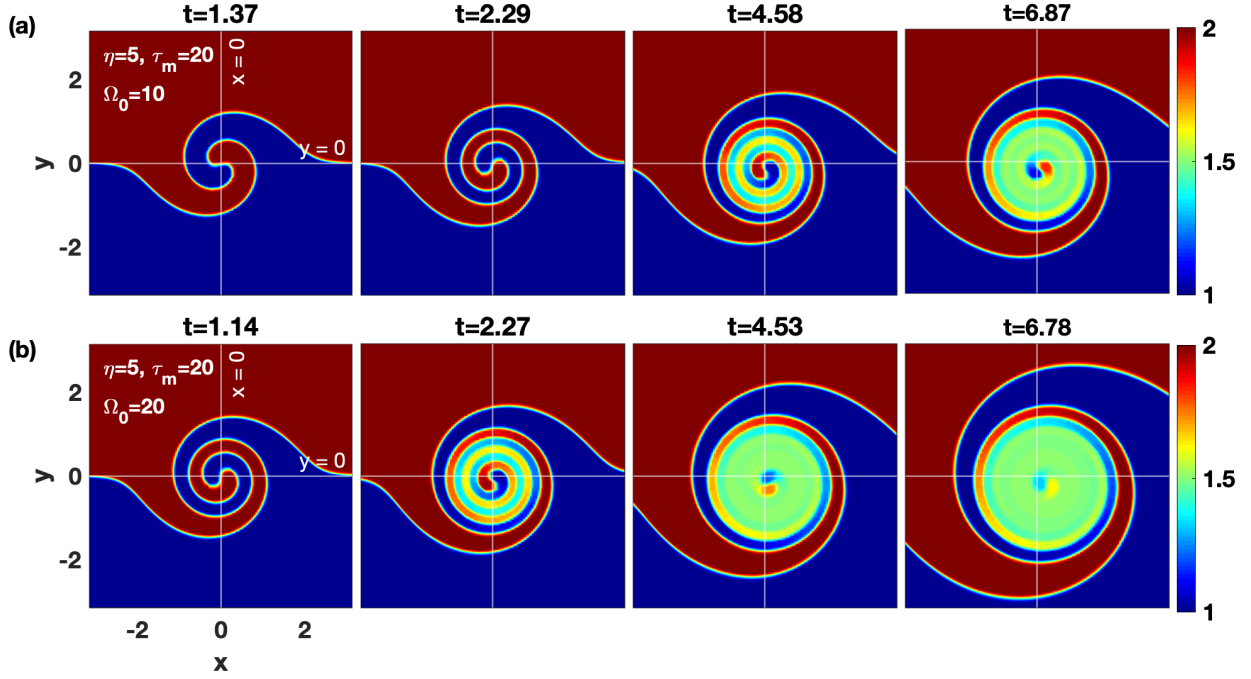


FIG. 6. Time evolution of sharp density profile for strongly coupled dusty plasma medium, where $\eta=5$; $\tau_m=20$. (a) $\Omega_0 = 10$ and (b) $\Omega_0 = 20$. The expansion rate (radial velocity) is high and the number of turns (angular velocity) of the spiral arms are almost double in (b) in comparison to (a) due to the two times of the angular velocity. Furthermore, the spiral arms of both densities (lighter and denser) are distinguishable in the early time while later get smeared out.

Spiral waves have both angular as well as radial velocity components. A comparison between Fig. 6(a) ($\Omega_0 = 10$) and Fig. 6(b) ($\Omega_0 = 20$) shows that the expansion rate (radial velocity) is high and the number of turns (angular velocity) of the spiral arms are almost double in Fig. 6(b) in comparison to Fig. 6(a) due to the two times of the angular velocity. Thus, the conclusion is that the number of turns of spiral arms are proportional to the amplitude of vorticity. Furthermore, the spiral arms of both densities (lighter and denser) are distinguishable in the early time while later get smeared out. So far, we have dealt with a medium having two fluids of different densities which results in the formation of two kind of spiral arms. Next we have simulated a medium has four fluids of different densities over the rotating coherent structure as shown in Figure 7. The boundary conditions have been taken care of by considering all the four density quadrants are localised and lie inside the density region considered in Fig. 1(a).

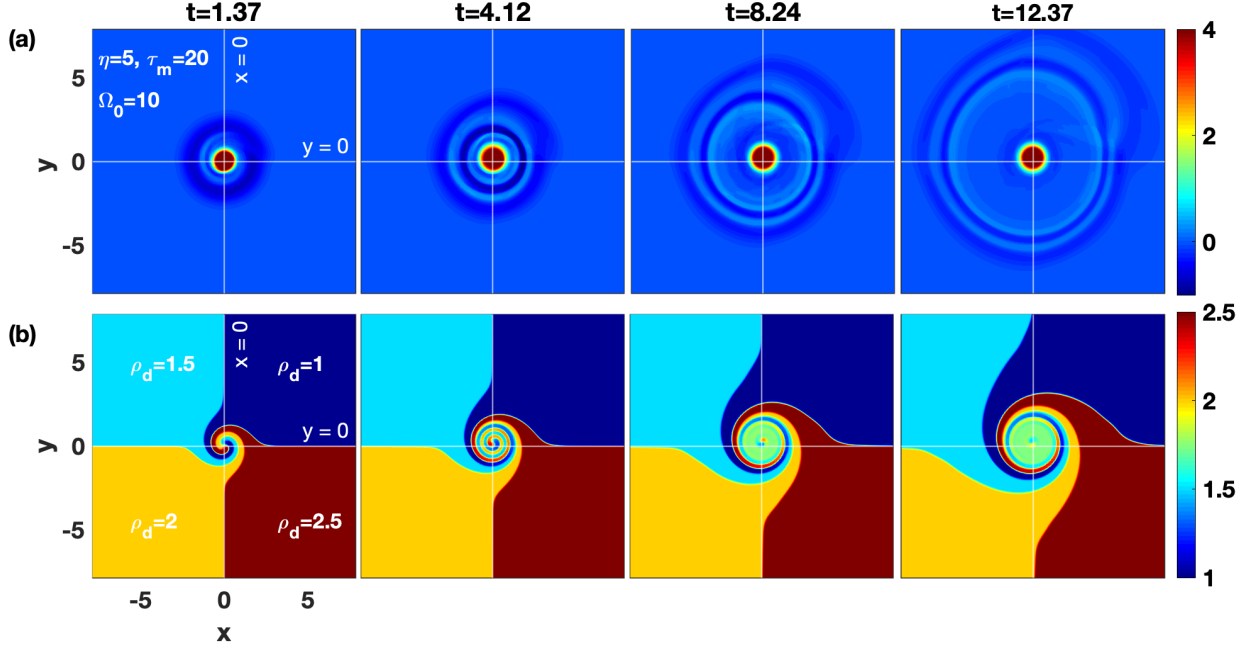


FIG. 7. Time evolution of four different sharp densities profiles over the rotating coherent structure for SCDPs for the $\eta=5$; $\tau_m=20$. In (a) colorbar designates the vorticity. It can be noticed: The greater the density/ Γ of the medium, the steeper the TS waves; the lighter the density of a medium, the faster the speed of TS waves; the speed difference in different quadrants and the density gradient cause the wavefronts are no longer cylindrical symmetric around the center of rotation and the shift in the vorticity center towards the low density quadrant and, in (b) four distinguishable spiral arms for each of density is observed in the early time while later get smeared out; colorbar shows the density.

Again from Fig. 7 it can be noticed: The greater the density/ Γ of the medium, the steeper the TS waves; the lighter the density of a medium, the faster the speed of TS waves; the speed difference in different quadrants and the density gradient cause the wavefronts are no longer cylindrical symmetric around the center of rotation and the shift in the vorticity center towards the low density quadrant. In Fig. 7(b) four distinguishable spiral arms for each of density is observed in the early time while later get smeared out. Thus, from all the above evolutions of the density profiles it can be anticipated that the number spiral arms are proportional to the number of different densities coexist over the smooth rotating structure.

B. Rigid rotating vortex

Thus far, we had specifically avoided the development of fluid Kelvin-Helmholtz (KH) instability by taking smooth flow profiles. Here, we take vorticity profile B with a sharp cut-off (first snapshot at $t = 0$ in Figs. 8(a) and 9(a)) i.e. setting the vorticity $\xi_{z0} = 0$ beyond $r = r_0 (= 6.0)$ and for $r \leq r_0$ the vorticity is taken to have a constant value $\xi_{z0} = 2\phi_0$; $\phi_0=1$. Another possibility which we explored in our previous paper⁵³ was the evolution of the same sharp cut-off rotating vortex in the SCDPs with constant background density. In the present paper, we introduce an additional density inhomogeneity where $\rho_d=1$ (lighter) for $-6\pi \leq y \leq 0$ and $\rho_d=2$ (denser) for $0 = y \leq 6\pi$ (first snapshot at $t = 0$ in Figs. 8(b) and 9(b)). For the HD system, it is evident from the Fig. 8 that turning on the vortex the abruptness of vorticity profile generates a strong rotational sheared flow, which in turn is drastically unstable to the KH instability leads to the creation of small KH vortices across the vorticity interface and after that as time progresses the merging of these vortices takes place. This creation and merging process of KH vortices distorts the formation of the spiral waves around the rotor.

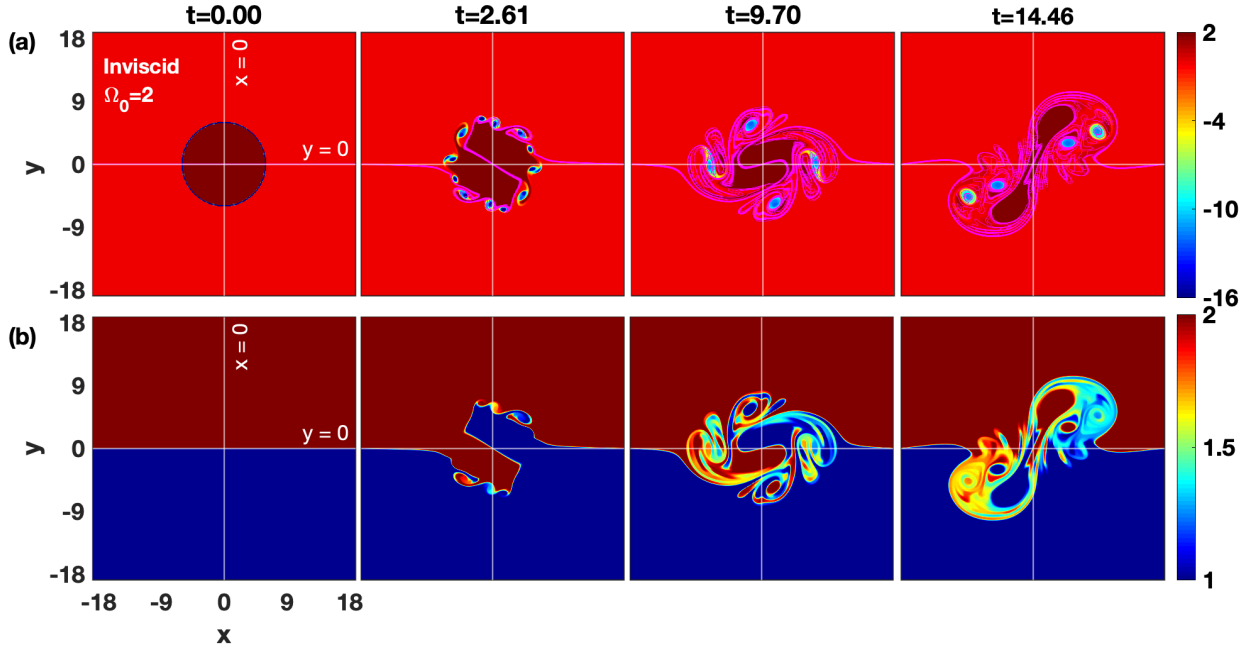


FIG. 8. Time evolution of a sharp counter-rotating vorticity profile ($\Omega_0 = 10$) in an inviscid HD fluid ($\eta=5$; $\tau_m=20$) with background density inhomogeneity along the interface $y=0$. (a) Evolution of a sharp counter-rotating vorticity, where the magenta color solid line is just the interface of respective density profile and (b) density profile evolution

We know that an incompressible GHD system, besides KH instability, also favours the TS waves emission. In Fig. 9(a) where $\eta=5$; $\tau_m=20$, we observe a pair of ingoing and outgoing wavefronts emanates from the interface and a concomitant KH destabilization at each of these fronts.

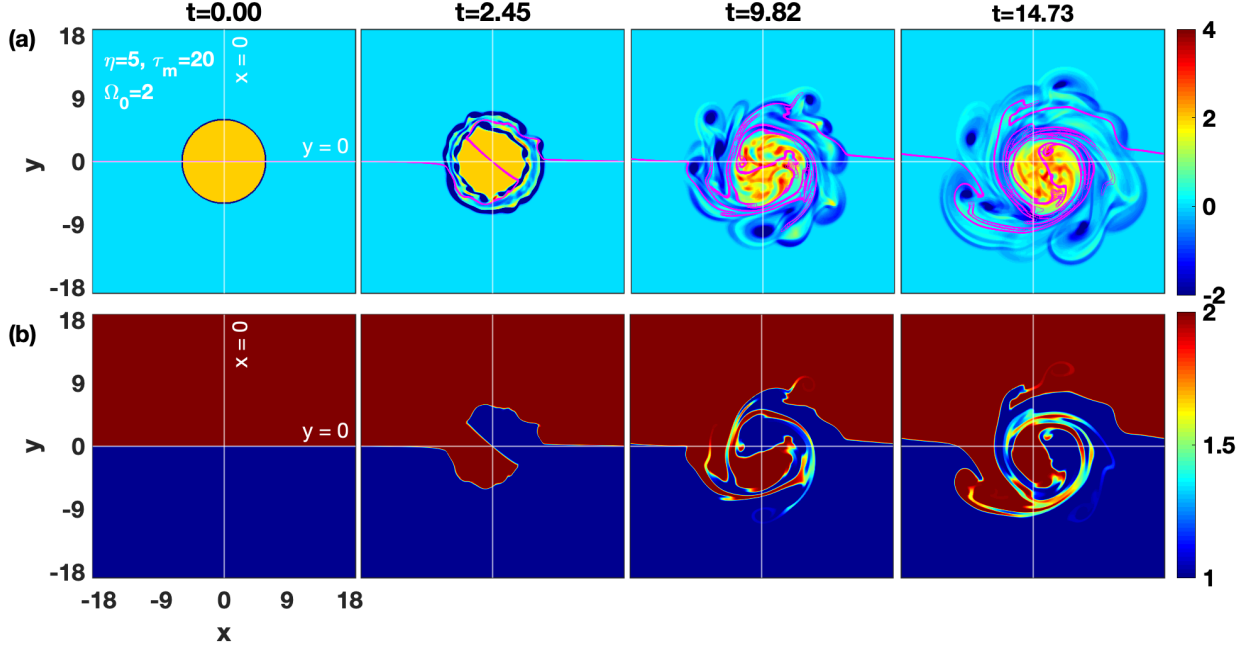


FIG. 9. Time evolution of a sharp counter-rotating vorticity for GHD system where $\eta=5$; $\tau_m=20$ with sharp background density inhomogeneity along the interface $y=0$. (a) Evolution of a sharp vorticity is $\xi_{z0} = 0$ beyond $r = r_0 (= 6.0)$ and for $r \leq r_0$ the vorticity is taken to have a constant value $\xi_{z0} = 2\phi_0$; $\phi_0=1$, where the magenta color solid line is just the interface of respective density profile and (b) density profile evolution.

The response of the respective background fluid density to the rigid rotor (Fig. 9(a)) is shown in Fig. 9(b) where as soon as the rotor begins to rotate: initially, the fluid within the inner region ($|r| \leq 6$) starts rotating with it which later on undergoes mixing due to the ingoing wave from the interface while the stagnant fluid in the outer region ($|r| \geq 6$) undergoes mixing due to the outgoing wave from the interface, and the fluid near the interface starts binding around it. The interplay between the ingoing and outgoing wavefronts, and KH instability distorts the formation of spiral waves around the rotor. But here, the TS waves are help in efficient mixing of the viscoelastic fluids by convecting the fluids inside and outside the vortex structure. Additionally, as the TS waves travel faster in lower density part than upper density part and the density gradient cause the counter rotating vorticity center gets shifted towards the low density side while a HD fluid does not

support any TS wave so there is no shifting in the center of rotation. Here, it should be noted that the HD results are used only to facilitate the understanding of our observations of GHD system not for any comparative analysis.

IV. CONCLUSIONS AND OUTLOOK

Dusty plasmas support the long-lived coherent structures which can provide a driving force for the generation of different types of waves and instabilities. Here, we have examined how the density heterogeneity in dusty plasmas responds to the circularly rotating vortex monopoles, namely smooth and sharp cut-off. We have carried out the 2D fluid simulations in the framework of generalized hydrodynamics fluid model. A fluid description is applicable if all spacial scales being considered are about an order of magnitude larger than the interparticle distance. The rotating vortices are placed at the interface of different densities. The smooth rotating vortex causes to form the spiral density waves and radial emission of TS waves into the surrounding media according to the shear wave speed. It is noticed that the spiral density waves are distinguishable in the early time while later get smeared out. Spiral waves are observed in many biological, physical, and chemical systems⁶¹⁻⁶⁵. A sharp rotating vortex favors the Kelvin-Helmholtz (KH) instability across its interface. In such flows for the GHD system, the interplay between the emitted TS waves and the vortices of KH instability distorts the formation of the regular spiral density arms around the rotor. It is observed that the TS waves play an important role in controlling the transport properties like mixing, and diffusion. Although, here, the density inhomogeneity has been introduced hypothetically (in order to identify the TS waves) for simulation but the presented results can be easily generalized to any typical SCDP experiment having realistic density inhomogeneity *e.g.*, sech type, parabolic type, etc. and by locating the driving vortex at the required place. In 3D system the TS waves may be less effective because the amplitude of an emerging TS wave from a spherical source will decrease faster ($1/r$) than the present 2D case (here, $1/\sqrt{r}$). Also, here, we have only explored a rotating coherent vorticity structures specifically, smooth and sharp cut-off. It would also be interesting to see the evolution of such inhomogeneous media having other types of coherent structures like elliptical, dipole, and tripole.

REFERENCES

- ¹Anatoli Tur and Vladimir Yanovsky. *Coherent Vortex Structures in Fluids and Plasmas*. Springer, 2017.
- ²Louis F Rossi, Joseph F Lingeitch, and Andrew J Bernoff. Quasi-steady monopole and tripole attractors for relaxing vortices. *Physics of Fluids*, 9(8):2329–2338, 1997.
- ³Ziv Kizner and Ruvim Khvoles. The tripole vortex: Experimental evidence and explicit solutions. *Physical Review E*, 70(1):016307, 2004.
- ⁴Thomas Leweke, Stéphane Le Dizes, and Charles HK Williamson. Dynamics and instabilities of vortex pairs. *Annual Review of Fluid Mechanics*, 48:507–541, 2016.
- ⁵Michael J Lighthill and James Lighthill. *Waves in fluids*. Cambridge university press, 2001.
- ⁶NN Rao, PK Shukla, and M Yu Yu. Dust-acoustic waves in dusty plasmas. *Planetary and space science*, 38(4):543–546, 1990.
- ⁷Mangilal Choudhary, S Mukherjee, and P Bandyopadhyay. Propagation characteristics of dust-acoustic waves in presence of a floating cylindrical object in the dc discharge plasma. *Physics of Plasmas*, 23(8):083705, 2016.
- ⁸John Grove. The interaction of shock waves with fluid interfaces. *Advances in Applied Mathematics*, 10(2):201–227, 1989.
- ⁹Douglas Rotman. Shock wave effects on a turbulent flow. *Physics of Fluids A: Fluid Dynamics*, 3(7):1792–1806, 1991.
- ¹⁰Wei Lin, MS Murillo, and Yan Feng. Pressure and energy of compressional shocks in two-dimensional yukawa systems. *Physical Review E*, 100(4):043203, 2019.
- ¹¹Shigeki Imao, Motoyuki Itoh, Yutaka Yamada, and Qiming Zhang. The characteristics of spiral waves in an axially rotating pipe. *Experiments in fluids*, 12(4-5):277–285, 1992.
- ¹²Dwight Barkley. Linear stability analysis of rotating spiral waves in excitable media. *Physical Review Letters*, 68(13):2090, 1992.
- ¹³FM Peeters and Xiaoguang Wu. Wigner crystal of a screened-coulomb-interaction colloidal system in two dimensions. *Physical Review A*, 35(7):3109, 1987.
- ¹⁴SV Vladimirov, PV Shevchenko, and NF Cramer. Vibrational modes in the dust-plasma crystal. *Physical Review E*, 56(1):R74, 1997.
- ¹⁵P Schmidt, G Zwicknagel, P-G Reinhard, and C Toepffer. Longitudinal and transversal collective modes in strongly correlated plasmas. *Physical Review E*, 56(6):7310, 1997.

- ¹⁶Xiaogang Wang, Amitava Bhattacharjee, and S Hu. Longitudinal and transverse waves in yukawa crystals. *Physical review letters*, 86(12):2569, 2001.
- ¹⁷MS Murillo. Critical wave vectors for transverse modes in strongly coupled dusty plasmas. *Physical review letters*, 85(12):2514, 2000.
- ¹⁸Bin Liu, K Avinash, and John Goree. Transverse optical mode in a one-dimensional yukawa chain. *Physical review letters*, 91(25):255003, 2003.
- ¹⁹P. G. Drazin. Kelvin–helmholtz instability of finite amplitude. *Journal of Fluid Mechanics*, 42(2):321–335, 1970.
- ²⁰S Chandrasekhar. Hydrodynamic and hydromagnetic stability, dover, new york, 1981.
- ²¹Lord Rayleigh. Investigation of the character of the equilibrium of an incompressible heavy. 1900.
- ²²Geoffrey Ingram Taylor. The instability of liquid surfaces when accelerated in a direction perpendicular to their planes. i. *Proceedings of the Royal Society of London. Series A. Mathematical and Physical Sciences*, 201(1065):192–196, 1950.
- ²³H Thomas, GE Morfill, V Demmel, J Goree, B Feuerbacher, and D Möhlmann. Plasma crystal: Coulomb crystallization in a dusty plasma. *Physical Review Letters*, 73(5):652, 1994.
- ²⁴Edward Thomas Jr. Direct measurements of two-dimensional velocity profiles in direct current glow discharge dusty plasmas. *Physics of plasmas*, 6(7):2672–2675, 1999.
- ²⁵R Ichiki, Yu Ivanov, M Wolter, Y Kawai, and A Melzer. Melting and heating of two-dimensional coulomb clusters in dusty plasmas. *Physical Review E*, 70(6):066404, 2004.
- ²⁶Zach Haralson and John Goree. Laser heating of 2-d dusty plasmas using a random arc pattern. *IEEE Transactions on Plasma Science*, 44(4):549–552, 2015.
- ²⁷Zach Haralson and J Goree. Temperature dependence of viscosity in a two-dimensional dusty plasma without the effects of shear thinning. *Physics of Plasmas*, 23(9):093703, 2016.
- ²⁸Andre Melzer, Harald Krueger, Stefan Schuett, and Matthias Mulsow. Finite dust clusters under strong magnetic fields. *Physics of Plasmas*, 26(9):093702, 2019.
- ²⁹Anton Kananovich and J Goree. Experimental determination of shock speed versus exciter speed in a two-dimensional dusty plasma. *Physical Review E*, 101(4):043211, 2020.
- ³⁰A Piel, V Nosenko, and J Goree. Laser-excited shear waves in solid and liquid two-dimensional dusty plasmas. *Physics of plasmas*, 13(4):042104, 2006.
- ³¹Yan Feng, Wei Lin, Wei Li, and Qiaoling Wang. Equations of state and diagrams of two-dimensional liquid dusty plasmas. *Physics of Plasmas*, 23(9):093705, 2016.

- ³²Peter Hartmann, Jorge C Reyes, Evdokiya G Kostadinova, Lorin S Matthews, Truell W Hyde, Ranna U Masheyeva, Karlygash N Dzhumagulova, Tlekkabul S Ramazanov, Torben Ott, Hanno Kählert, et al. Self-diffusion in two-dimensional quasimagnetized rotating dusty plasmas. *Physical Review E*, 99(1):013203, 2019.
- ³³Wei Lin, MS Murillo, and Yan Feng. Universal relationship of compression shocks in two-dimensional yukawa systems. *Physical Review E*, 101(1):013203, 2020.
- ³⁴J. Frenkel. *Kinetic Theory Of Liquids*. Dover Publications, 1955.
- ³⁵S Nunomura, J Goree, S Hu, X Wang, and Amitava Bhattacharjee. Dispersion relations of longitudinal and transverse waves in two-dimensional screened coulomb crystals. *Physical Review E*, 65(6):066402, 2002.
- ³⁶S Nunomura, S Zhdanov, D Samsonov, and G Morfill. Wave spectra in solid and liquid complex (dusty) plasmas. *Physical review letters*, 94(4):045001, 2005.
- ³⁷István Donkó, Peter Hartmann, and Zoltán Donkó. Molecular dynamics simulation of a two-dimensional dusty plasma. *American Journal of Physics*, 87(12):986–993, 2019.
- ³⁸P. K. Kaw and A. Sen. Low frequency modes in strongly coupled dusty plasmas. *Physics of Plasmas*, 5(10):3552–3559, 1998.
- ³⁹P. K. Kaw. Collective modes in a strongly coupled dusty plasma. *Physics of Plasmas*, 8(5):1870–1878, 2001.
- ⁴⁰S Nunomura, D Samsonov, and J Goree. Transverse waves in a two-dimensional screened-coulomb crystal (dusty plasma). *Physical review letters*, 84(22):5141, 2000.
- ⁴¹J Pramanik, G Prasad, A Sen, and PK Kaw. Experimental observations of transverse shear waves in strongly coupled dusty plasmas. *Physical review letters*, 88(17):175001, 2002.
- ⁴²P Bandyopadhyay, G Prasad, A Sen, and PK Kaw. Driven transverse shear waves in a strongly coupled dusty plasma. *Physics Letters A*, 372(33):5467–5470, 2008.
- ⁴³Amruta Mishra, PK Kaw, and A Sen. Instability of shear waves in an inhomogeneous strongly coupled dusty plasma. *Physics of Plasmas*, 7(8):3188–3193, 2000.
- ⁴⁴G Sorasio, PK Shukla, and DP Resendes. Instability of shear waves in a nonuniform dusty plasma. *New Journal of Physics*, 5(1):81, 2003.
- ⁴⁵Sandeep Kumar and Amita Das. Spiral waves in driven strongly coupled yukawa systems. *Physical Review E*, 97(6):063202, 2018.
- ⁴⁶Sandeep Kumar, Bhavesh Patel, and Amita Das. Spiral waves in driven dusty plasma medium: Generalized hydrodynamic fluid description. *Physics of Plasmas*, 25(4):043701, 2018.

- ⁴⁷Ligang Li, Xinhao Liao, Kit H Chan, and Keke Zhang. On nonlinear multiarmed spiral waves in slowly rotating fluid systems. *Physics of Fluids*, 22(1):011701, 2010.
- ⁴⁸NA Gorelova and J Bureš. Spiral waves of spreading depression in the isolated chicken retina. *Journal of neurobiology*, 14(5):353–363, 1983.
- ⁴⁹Jorge M Davidenko, Arcady V Pertsov, Remy Salomonsz, William Baxter, and José Jalife. Stationary and drifting spiral waves of excitation in isolated cardiac muscle. *Nature*, 355(6358):349–351, 1992.
- ⁵⁰James Lechleiter, Steven Girard, Ernest Peralta, and David Clapham. Spiral calcium wave propagation and annihilation in xenopus laevis oocytes. *Science*, 252(5002):123–126, 1991.
- ⁵¹Hiroyuki Kitahata and Masanobu Tanaka. Mathematical approach to unpinning of spiral waves anchored to an obstacle with high-frequency pacing. *Biophysics and physcobiology*, 15:196–203, 2018.
- ⁵²Debra Meloy Elmegreen. A near-infrared atlas of spiral galaxies. *The Astrophysical Journal Supplement Series*, 47:229–233, 1981.
- ⁵³V. S. Dharodi, S. K. Tiwari, and A. Das. Visco-elastic fluid simulations of coherent structures in strongly coupled dusty plasma medium. *Physics of Plasmas*, 21(7):073705, 2014.
- ⁵⁴Abdourahmane Diaw and Michael Sean Murillo. Generalized hydrodynamics model for strongly coupled plasmas. *Physical Review E*, 92(1):013107, 2015.
- ⁵⁵V. S. Dharodi, A. Das, B. G. Patel, and P. K. Kaw. Sub-and super-luminar propagation of structures satisfying poynting-like theorem for incompressible generalized hydrodynamic fluid model depicting strongly coupled dusty plasma medium. *Physics of Plasmas*, 23(1):013707, 2016.
- ⁵⁶Setsuo Ichimaru, Hiroshi Iyetomi, and Shigenori Tanaka. Statistical physics of dense plasmas: thermodynamics, transport coefficients and dynamic correlations. *Physics Reports*, 149(2-3):91–205, 1987.
- ⁵⁷Nada Sekeljic. Asymptotic expansion of bessel functions; applications to electromagnetics. *Dynamics at the Horsetooth*, 2, 2010.
- ⁵⁸J. P. Boris, A. M. Landsberg, E. S. Oran, and J. H. Gardner. *LCPFCT A flux-corrected transport algorithm for solving generalized continuity equations*. Technical Report NRL Memorandum Report 93-7192, Naval Research Laboratory, 1993.
- ⁵⁹P Swarztrauber, R Sweet, and John C Adams. Fishpack: Efficient fortran subprograms for the solution of elliptic partial differential equations. *UCAR Publication*, July, 1999.

- ⁶⁰Hiroyuki Ikezi. Coulomb solid of small particles in plasmas. *The Physics of fluids*, 29(6):1764–1766, 1986.
- ⁶¹MA Allesie, FIM Bonke, and FJG Schopman. Circus movement in rabbit atrial muscle as a mechanism of tachycardia: II. *Circ Res*, 39:168–177, 1976.
- ⁶²G t Gerisch. Stadienspezifische aggregationsmuster bei dictyostelium discoideum. *Wilhelm Roux'Archiv fur Entwicklungsmechanik der Organismen*, 156(2):127–144, 1965.
- ⁶³Eberhard Bodenschatz, John R de Bruyn, Guenter Ahlers, and David S Cannell. Transitions between patterns in thermal convection. *Physical review letters*, 67(22):3078, 1991.
- ⁶⁴Marta Net, Isabel Mercader, and Edgar Knobloch. Binary fluid convection in a rotating cylinder. *Physics of Fluids*, 7(7):1553–1567, 1995.
- ⁶⁵K Agladze and O Steinbock. Waves and vortices of rust on the surface of corroding steel. *The Journal of Physical Chemistry A*, 104(44):9816–9819, 2000.